Structures 43 (2022) 1369–1379

Contents lists available at ScienceDirect

Structures

journal homepage: www.elsevier.com/locate/structures

Seismic performance of prefabricated semi-rigid RCS structures

Zhihong Pan [a], Qi Si [b,*], Yanzhang Zhu [c], Hui Ying [c], Xingxing Wang [c], Dingfa Du [d]

[a] School of Civil Engineering and Architecture, Jiangsu University of Science and Technology, Zhenjiang 212003, China
[b] School of Civil Engineering, Tianjin University, Tianjin 300072, China
[c] School of Civil Engineering and Architecture, Jiangsu University of Science and Technology, Zhenjiang 212003, China
[d] College of Water Conservancy and Hydropower Engineering, Hohai University, Nanjing 210000, China

ARTICLE INFO

Keywords:
Prefabricated structure
RCS joint
Seismic performance
Semi-rigid connection
Moment-rotation
Dynamic elastic–plastic analysis

ABSTRACT

To study the seismic behavior of prefabricated reinforced concrete column-steel beam (RCS) hybrid structures, a cyclic loading test on a novel RCS joint was conducted to investigate the failure modes, ductility, and energy dissipation. The moment-rotation relationship model of the joint was proposed according to the test. Furthermore, the model of a 3-bay, 5-story semi-rigid prefabricated RCS frame was established in SAP2000 software. The modal analysis and dynamic elastic–plastic analysis were carried out on the semi-rigid and rigid RCS frames respectively to study the effect of semi-rigid connections on the seismic performance of RCS structures. Analysis results show that the failure mode of the prefabricated RCS joint meets the strong column-weak beam requirement. The 'bow'-shaped hysteretic curve indicates the joint has good seismic performance with good ductility and energy dissipation capacity. Compared to rigid RCS structures, semi-rigid connections lead to a reduction in the overall stiffness and an increase in the natural vibration periods of the structure. Under the action of the earthquake, the base shear force of the semi-rigid RCS structure is smaller than that of the rigid RCS structure. The maximum inter-story drift angles and top displacement of semi-rigid RCS structures will increase, but still meet the requirements of the seismic standard.

1. Introduction

A composite frame consisting of reinforced concrete column and steel beam (RCS) is a new type of structure developed based on steel and reinforced concrete structures. The characteristics of the RCS structure mainly include the following four aspects. Firstly, the reinforced concrete with good compressive properties as the material of the columns can significantly increase the lateral stiffness of the structure and reduce the inter-story displacement angle. Secondly, the reinforced concrete columns have excellent fire and corrosion resistance, which can further reduce the cost of material and labor compared with steel columns. Thirdly, the steel beams have excellent tensile properties that can minimize the cross-sectional size and increase the span of the members. Finally, the smaller self-weight of steel beams can reduce the overall structural seismic effect, increase the seismic safety and ductility of the structure, and reduce the construction cost. Therefore, RCS frame structures were widely adopted in medium and high-rise buildings, large-span structures, and buildings with high seismic requirements.

In the last few decades, relevant research on RCS structures has been carried out widely [1,2]. The RCS connections could be broadly classified into two main categories, namely the beam-through type and the column-through type [3–5], as illustrated in Fig. 1.

Sheikh [6] examined the behavior of typically composite beam-column connections through the results of an experimental research program where 15 two-thirds scale joint specimens were tested under monotonic and cyclic loading. Alizadeh [7] designed two interior RCS connections based on the strong column-weak beam criterion to study the seismic performance of RCS connections. Nguyen [8] studied the seismic performance of a new type of exterior RCS connection, in which a steel profile embedded inside the RC column is directly welded to the steel beam, and tested a full-scale exterior hybrid joint under cyclic loading.

In the context of sustainable development, new developments have also occurred in RCS structures, which have evolved from traditional rigid structures to semi-rigid prefabricated structures. Doost and Khaloo [9] studied the steel web panel's influence on the seismic behavior of the proposed precast RCS connections. Zhang [10] investigated the seismic performance of a prefabricated high-strength concrete tube

* Corresponding author.
E-mail addresses: zhhpan@just.edu.cn (Z. Pan), siqi@tju.edu.cn (Q. Si), 1642250149@qq.com (Y. Zhu), 576513867@qq.com (H. Ying), wangxingxing1288@126.com (X. Wang), ddfj_180@sina.com (D. Du).

https://doi.org/10.1016/j.istruc.2022.07.033
Received 7 March 2022; Received in revised form 9 July 2022; Accepted 12 July 2022
Available online 31 July 2022
2352-0124/

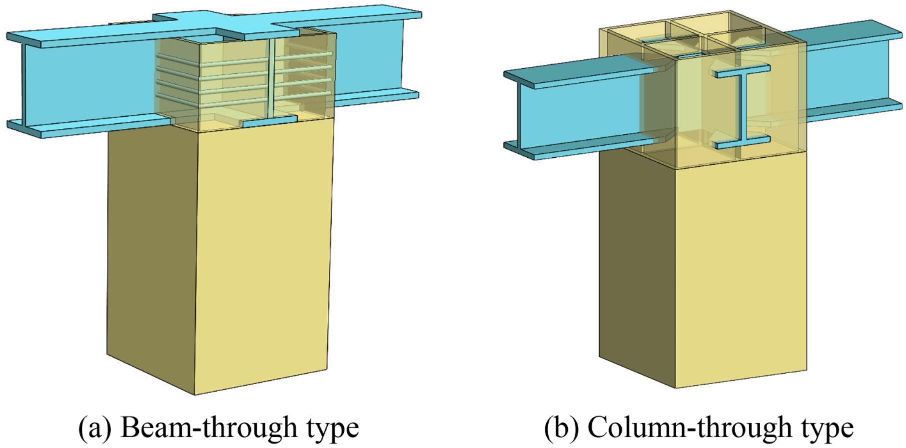

Fig. 1. RCS connections categories.

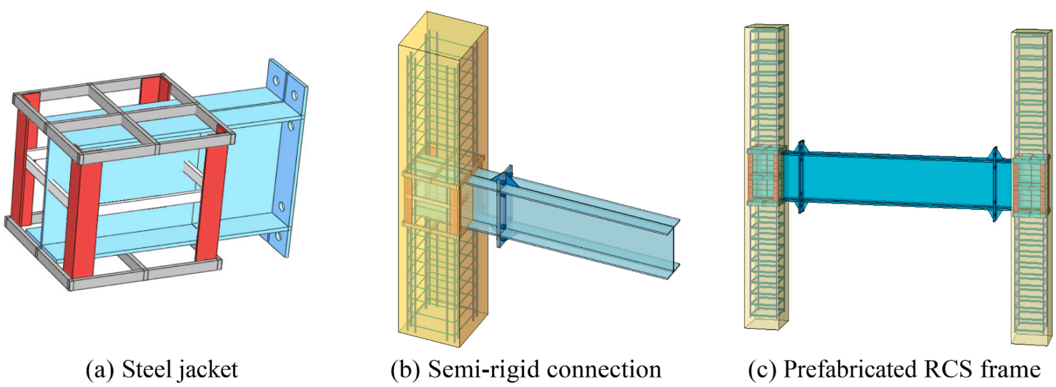

Fig. 2. Prefabricated RCS diagram.

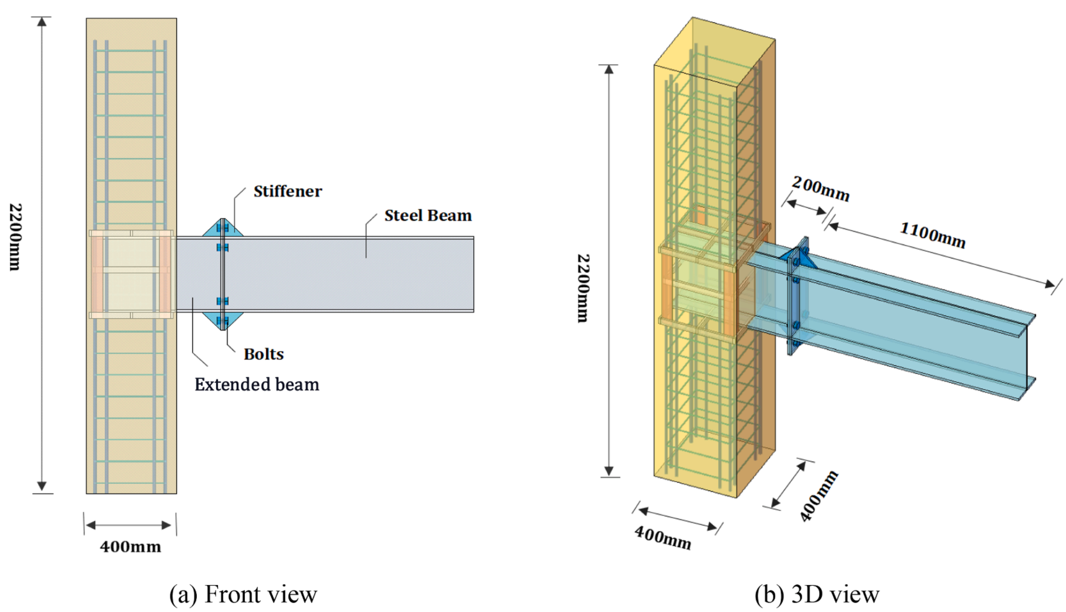

Fig. 3. Semi-rigid prefabricated RCS joint.

column–steel beam joint hybrid frame structure, a series of six full-scale joint specimens were tested under cyclic loading. Pan [11] proposed a new prefabricated semi-rigid connected RCS structural system based on the traditional RCS structure, which was composed of a steel jacket with an extended beam, concrete column, and steel beam. The steel jacket with extended beam was embedded in the concrete column, and the steel beam and extended beam were connected by endplate, as shown in Fig. 2. Si and Pan [12] analyzed the effects of different endplate

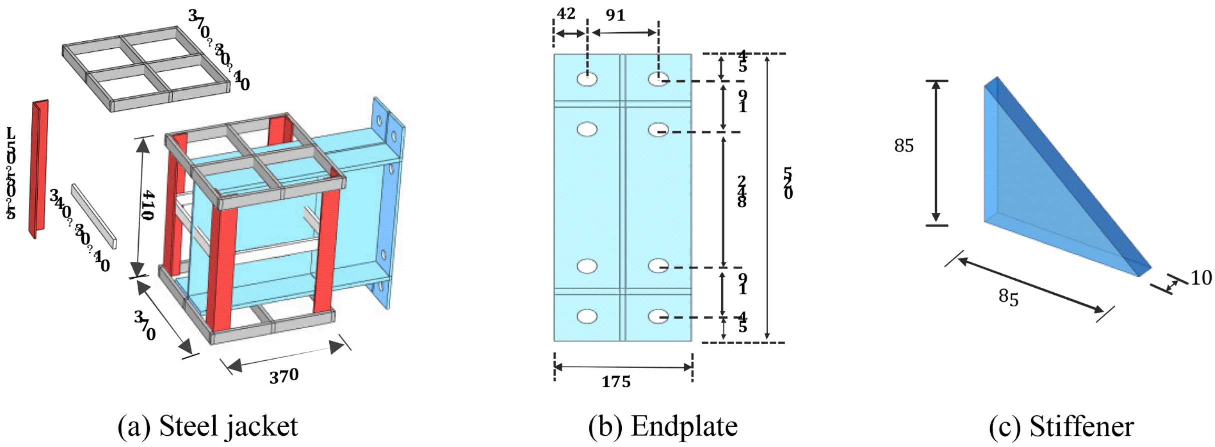

Fig. 4. Components in the joint.

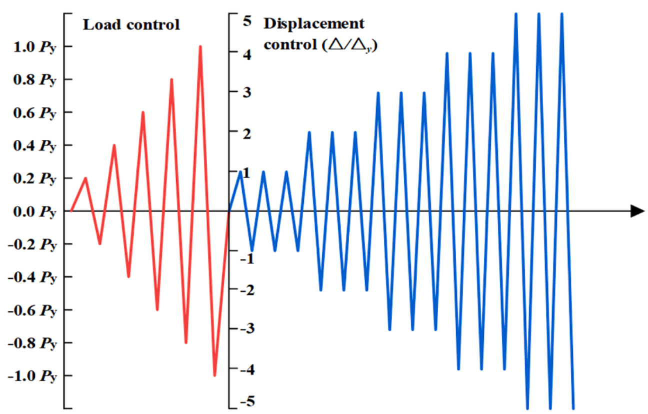

Fig. 5. Loading history.

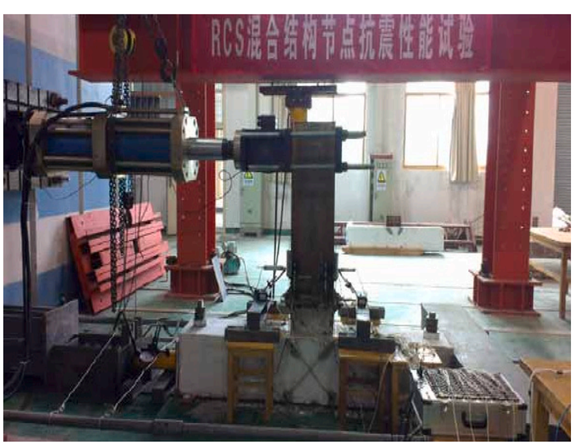

Fig. 6. Test diagram.

thicknesses, stiffening rib thicknesses, stiffening rib forms, and grades of high-strength bolt on the mechanical behavior and fire resistance of the semi-rigid prefabricated joint with the finite element software ABAQUS.

Above all, the existing research is more about the traditional RCS structure, but for the prefabricated RCS structure, the current research mostly focuses on the connection form of the joints, while the research about the seismic performance of the overall prefabricated RCS structure is inadequate. In this paper, based on the test of prefabricated RCS joints, the theoretical model of the moment rotation hysteresis curve of the semi-rigid RCS joints was established. The analytical model of a 3-bay, 5-story semi-rigid fabricated RCS frame was established in SAP2000 software, and the modal analysis and dynamic time history analysis were carried out on the semi-rigid and rigid RCS frames respectively, to study the effect of semi-rigid connections on the seismic performance of RCS structures.

2. Experimental study of the prefabricated RCS joint

2.1. Specimen design

The prefabricated RCS joint is mainly composed of a reinforced concrete column, steel beam, steel jacket with extended beam, and stiffening ribs, as shown in Fig. 3. To fully utilize the advantages of the RCS structural system, based on the end-plate connection, the extensional part of the joint was designed as a semi-rigid connection [13,14]. By weakening the connection, the plastic hinge will first appear at the joint, thus forming the yield mechanism of "strong column and weak beam". The stiffening ribs were set on both sides of the end plates to avoid premature buckling of the end plates at the connection [15]. The section size of the concrete column is 400 × 400 mm, the steel beam is HN350 × 175 × 7 × 11, and the length of the extended beam is 200 mm. The specific parameters of each component are shown in Fig. 4.

The force and displacement mixed loading method was adopted in the test, as shown in Fig. 5. In Fig. 5, P_y is the yield load, Δ is the loading displacement at the beam end, and Δy is the yield displacement [16]. Before yielding, the specimen was loaded by load control, with 20 % of yield load cyclic loading, once per stage. After yielding, the specimen was loaded by displacement control with multiple yield displacements as the step difference, and the displacement amplitude of each step was cycled three times [17]. The servo-hydraulic device was employed to load at the beam end of the specimen, as shown in Fig. 6.

2.2. Test results

During the test, when the horizontal displacement reached 12 mm, an initial crack was observed at the root of the steel beam, as shown in Fig. 7(a), and there was no crack in the joint core area. When loading to 24 mm, the endplate bent and yielded, as shown in Fig. 7(b). When loading to −42 mm, the weld of stiffener and beam flange fractured, and the endplate yielded significantly, as shown in Fig. 7(c). At the end of the loading, the stiffener at the opposite side was also pulled off, and the endplate was torn, as shown in Fig. 7(d).

The moment-rotation hysteretic curve of the joint is shown in Fig. 8 (a), and the shear-shear deformation (V-γ) hysteresis curve of the joint domain is shown in Fig. 8(b).

The results show that the joint has good energy dissipation capacity, and the maximum rotation is approximately 0.035 rad, which indicates

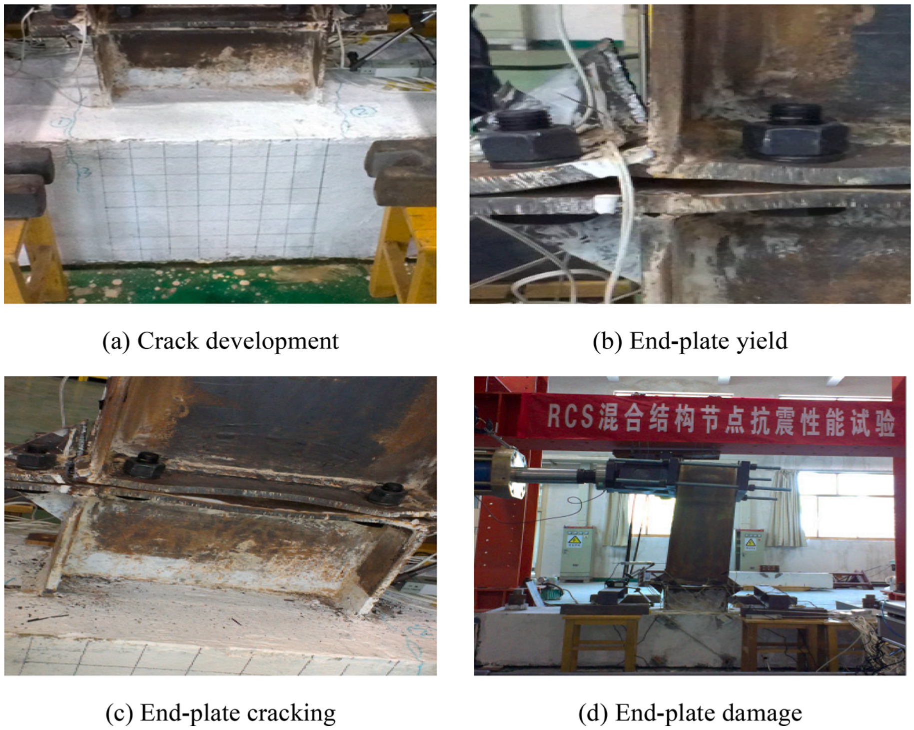

(a) Crack development (b) End-plate yield

(c) End-plate cracking (d) End-plate damage

Fig. 7. Failure of stiffener weld.

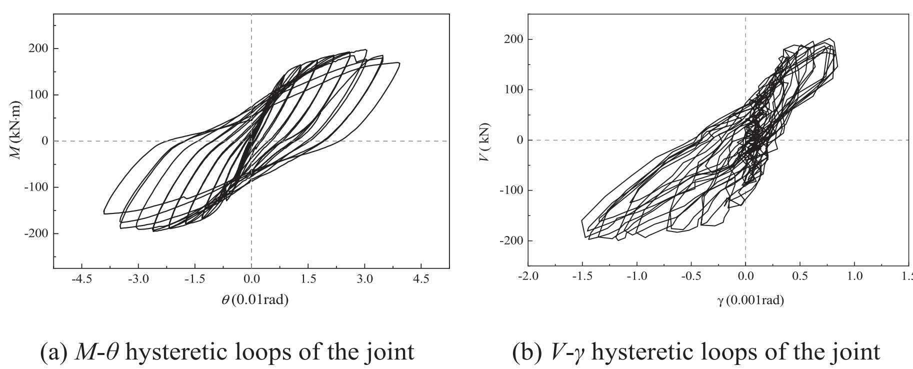

(a) M-θ hysteretic loops of the joint (b) V-γ hysteretic loops of the joint

Fig. 8. Results of the test.

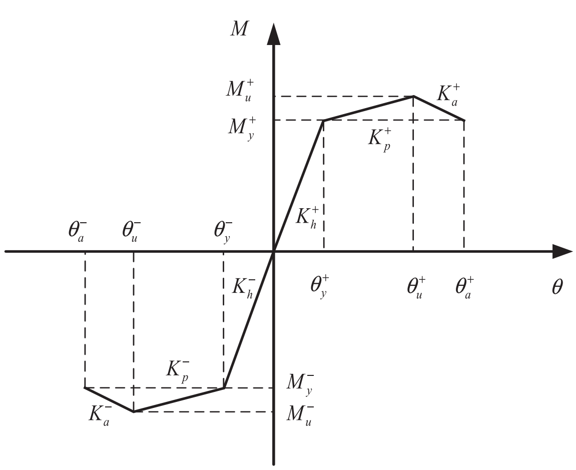

Fig. 9. Tri-linear skeleton curve.

that the joint has good rotation ability. The joint domain has no oblique crack, and the shear deformation is not obvious. The maximum shear angle of the joint domain is 0.0015 rad and the failure location was in the endplate, which satisfies the strong column-weak beam requirements [18]. Therefore, this paper argued that the steel jacket can provide high bearing capacity and stiffness for the joint core area, and the deformation and energy dissipation are mainly concentrated at the semi-rigid connections. The deformation of the joint is influenced mainly by the connection, and the influence of the joint core area could be neglected.

3. Moment rotation relationship model of prefabricated RCS joint

3.1. Skeleton curve

To evaluate the seismic performance of the prefabricated RCS frame structure, it is necessary to determine the theoretical analysis model of the semi-rigid behavior of prefabricated RCS joints. The models for the moment rotation relationship of semi-rigid joints contains linear,

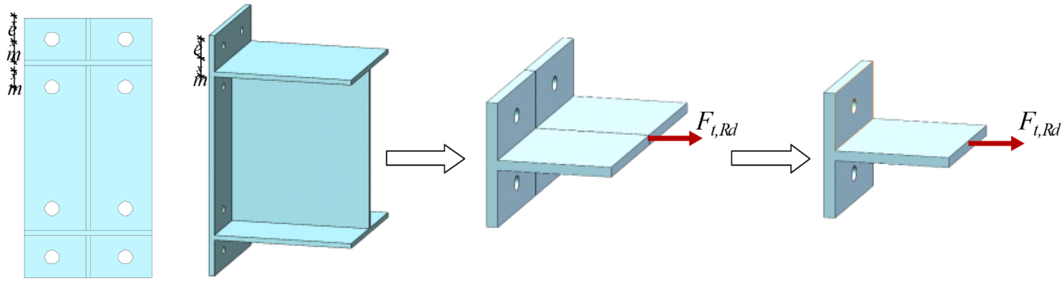

Fig. 10. Equivalent schematic diagram of *T*-connector.

Table 1
Calculated value of three key points.

Specimen	M_y (kN.m)	θ_y (rad)	M_u (kN.m)	θ_u (rad)	M_a (kN.m)	θ_a (rad)
Prefabricated RCS joint	167	0.0106	197	0.0293	167	0.0328

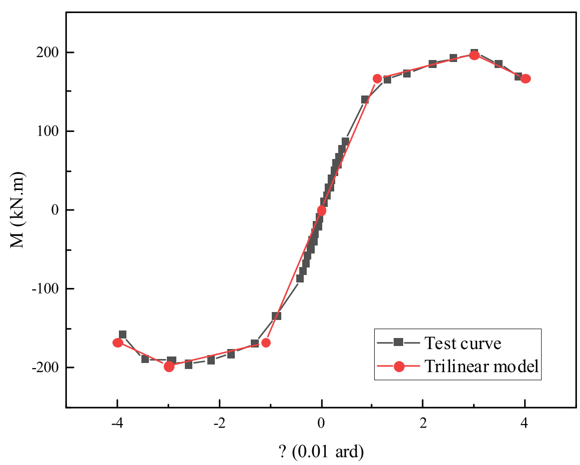

Fig. 11. Comparison chart of skeleton curve.

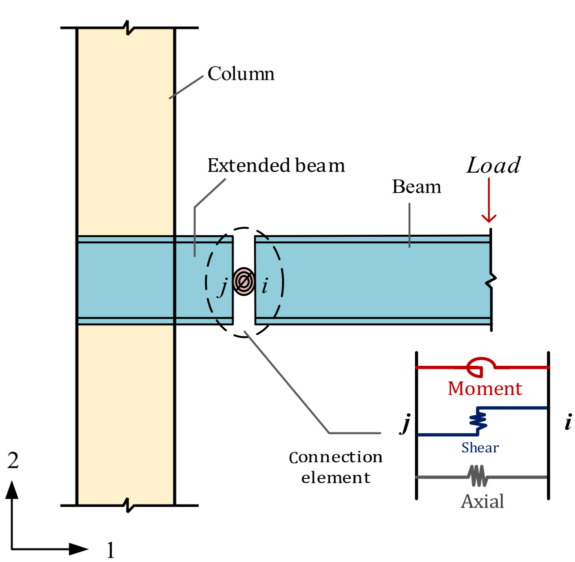

Fig. 12. Numerical simulation model.

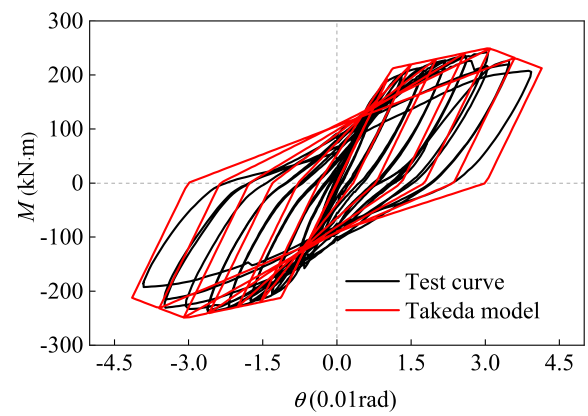

Fig. 13. Comparison of simulated and test curves.

polynomial, B-sample, and power models [19–22]. In this paper, based on the linear model, a tri-linear model of the moment-rotation curve applicable to the prefabricated RCS joint was proposed, as shown in Fig. 9.

The skeleton curve of the moment-rotation hysteretic model of the semi-rigid joint can be expressed as:

$$M = \begin{cases} K_h \cdot \theta & (0 \leqslant \theta \leqslant \theta_y) \\ M_y + K_p \cdot (\theta - \theta_y) & (\theta_y < \theta \leqslant \theta_u) \\ M_u + K_a \cdot (\theta - \theta_u) & (\theta_u < \theta \leqslant \theta_a) \end{cases} \quad (1)$$

where θ_y, θ_u, and θ_a represent the yield angle, limit angle, and maximum angle, respectively. M_y, M_u, and M_a are the yield moment, ultimate moment, and maximum moment, respectively. K_h, K_p, and K_a are the corresponding flexural rigidity, strain hardening stiffness, and descending stage stiffness, respectively.

In this paper, the stiffened end-plate bolted connection was adopted in the prefabricated semi-rigid RCS joint [23–25], the existing research shows that the thickness of the stiffener, the number of bolts have an impact on its mechanical properties, and the connection can be designed as rigid or semi-rigid. The component method was used to calculate the mechanical properties of the prefabricated semi-rigid RCS joint. The component method is a joint design method based on the mechanical model specified in Eurocode. In this method, the joint is divided into basic components and the spring model of the joint is established. The bearing capacity and stiffness of each component are calculated, and then the mechanical properties of the whole joint are obtained by assembling the spring model [26]. The connection part was specified as a *T*-stub [27,28], as shown in Fig. 11. The connection part was specified as a *T*-stub, as shown in Fig. 10. In this paper, there are four bolts at each of the upper and lower beam flanges, and the tensile load capacity (F_{bo}) provided by the bolts can be characterized as.

$$F_{bo} = 4A_{bo} \cdot f_{y.bo} \quad (2)$$

where A_{bo} is the cross-sectional area of a single bolt, $f_{y,bo}$ is the yield-

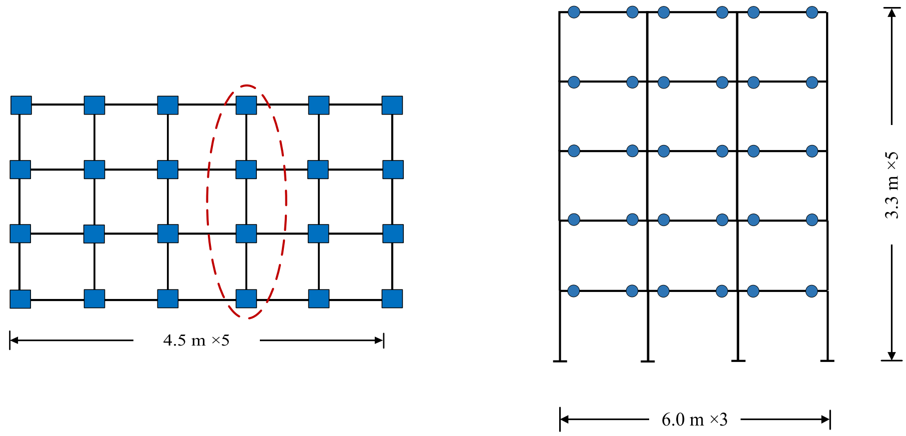

(a) Floor plan of the structure (b) Elevation of the structure

Fig. 14. Schematic diagram of the frame.

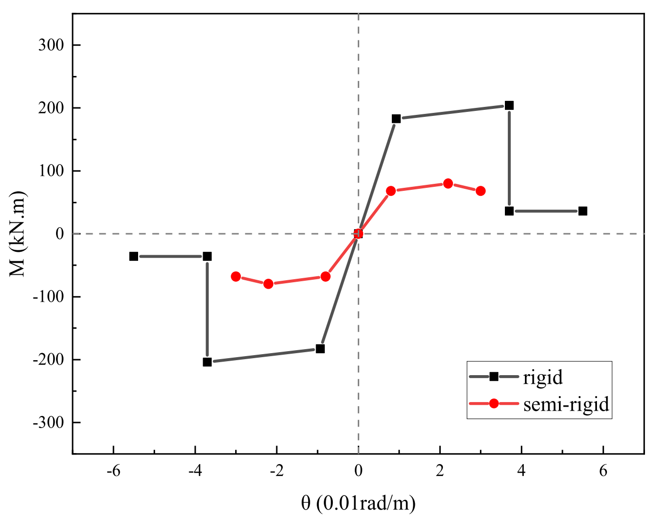

Fig. 15. Comparisons of skeleton curves.

Table 2
Natural vibration periods of structures (unit: s).

Models	Rigid RCS (T_1)	Semi-rigid RCS (T_2)	T_2 / T_1
1	1.144	1.357	1.186
2	0.295	0.325	1.102
3	0.126	0.132	1.048
4	0.071	0.073	1.028
5	0.060	0.061	1.017
6	0.057	0.060	1.053

bearing capacity of the bolt.

The tensile load capacity provided by the endplate can be expressed as

$$F_{t,Rd} = \frac{8M_{pl}}{m_x} \tag{3}$$

where M_{pl} is the flexural load capacity of the endplate equivalent to the T-stub,$M_{pl} = 0.25 l_{eff} t_c^2 f_y$. m_x is the geometric parameter, t_c is the thickness of the endplate; f_y is the yield strength of the endplate; l_{eff} is the length of the plastic hinge line of the endplate at ultimate damage, it can be calculated as$l_{eff} = \min(2\pi m_x, \pi m_x + 2e_x)$.

In summary, the ultimate flexural load capacity of the endplate and bolts can be calculated as

$$M_u = \min(F_{bo}, F_{t,Rd})\cdot h_e \tag{4}$$

where h_e is the effective height of the steel beam section.

Considering the effect of the stiffening ribs of the extended endplate, it is assumed that the stiffening ribs enter plasticity within 1/3 height, so the ultimate flexural bearing capacity of the assembled RCS joint can be approximated as.

$$M_u = \min(F_{bo}, F_{t,Rd})\cdot h_e + \frac{h_s}{3} t_{es} f_y \cdot (h_e + \frac{h_s}{6}) \tag{5}$$

where the h_s is the height of the stiffener; t_{es} is the thickness of the stiffener.

The initial rotational stiffness of prefabricated RCS joints was calculated using the component method in Europe code [29]. The initial rotational stiffness of the prefabricated RCS joint was contributed by the following four parts: flexural stiffness of the endplate and bolt tensile stiffness in the T-sub, tensile stiffness of the extended beam, compressive stiffness of the extended beam; and shear stiffness of the extended beam. The combination of endplates and bolts was equated to a T-sub subjected to tension, and the tensile stiffness provided by a single T-sub was approximated by

$$K_{ep}^{'} = \frac{1}{\frac{l_{ep}^3}{192 E_{ep} I_{ep}} + \frac{t_c}{11 E_{bo} A_{bo}}} \tag{6}$$

where E_{ep} and E_{bo} are the modulus of elasticity of the endplate and bolt respectively. A_{bo} is the effective tensile area of the bolt; t_c is the thickness of the endplate. I_{ep} is the moment of inertia of the endplate,$I_{ep} = l_{eff} t_c^3/12$. The endplates and bolts in the tension zone were equated to two T-subs, with the tensile stiffness can be expressed as

$$K_{ep} = \frac{1}{\frac{1}{K_{ep}^{'}} + \frac{1}{K_{ep}^{'}}} \tag{7}$$

Considering the effect of the stiffening ribs of the endplate, the stiffness of the endplate with stiffening ribs can be converted approximately according to the size of the web and the stiffening ribs [30], so the stiffness of the endplate with stiffening ribs can be determined by

$$K_{ep}^{+} = \frac{K_{ep}}{\mu} \tag{8}$$

where $\mu = A_w / (A_w + A_s)$, A_w and A_s are the areas of the web and stiffening ribs of the T-sub, respectively. μ = 1 when As = 0, corresponding to the case of no stiffening ribs.

Table 3
Comparison of natural vibration modes of structures.

Model	1st	2nd	3th	4th	5th	6th
Rigid RCS	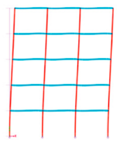	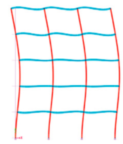	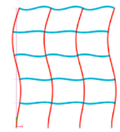	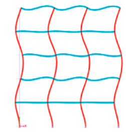	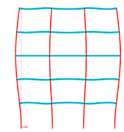	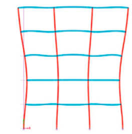
Semi-rigid RCS	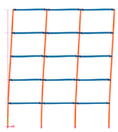	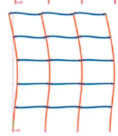	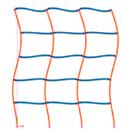	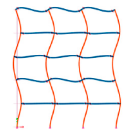	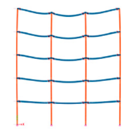	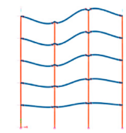

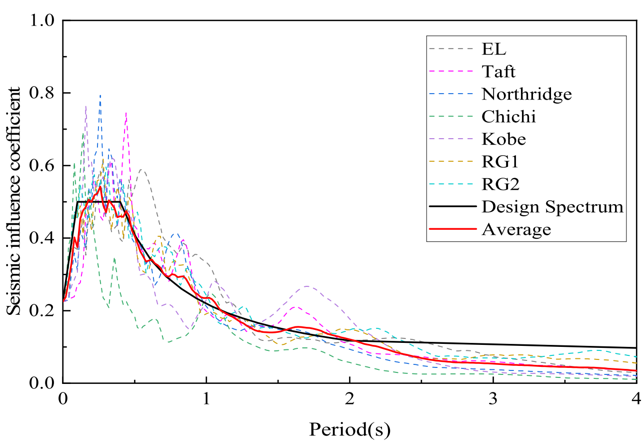

Fig. 16. The design scaled response spectra.

The compressive stiffness of the extended beam section is calculated in the same way as the tensile stiffness, which is approximated by

$$K_{cf,t} = \frac{Et_f b_f}{h_{cf}(1-\nu^2)} \tag{9}$$

where t_f, b_f, h_{cf} are the thickness and width of the flange of the extended beam and the extended distance, respectively. ν is the Poisson's ratio.

The shear stiffness of the web of the extended beam is approximated as

$$K_{cw,v} = 0.385\frac{EA_{v,cw}}{Z_{cw,v}} \tag{10}$$

where $A_{v,cw}$ is the shear area, $A_{v,cw} = h_{cf}{\cdot}t_{cw}$, t_{cw} is the thickness of the web, $Z_{cw,v}$ is the height of the web.

The stiffnesses provided by each component are listed above, and the relationship between the overall initial stiffness of the tensile zone and the stiffness of each component can be calculated by

$$\frac{1}{K_t} = \frac{1}{K_{ep}} + \frac{1}{K_{ep}} + \frac{1}{K_{cf,t}} \tag{11}$$

where K_{ep} is the endplate corresponding to the extended beam and frame beam respectively.

The total deformation of the semi-rigid prefabricated RCS joint was composed of the deformation of the tension zone at the connection (δ_t), the deformation of the compression zone (δ_c), and the shear deformation of the extended beam (δ_v). Therefore, the total deformation of the joint can be calculated by

$$\theta = \frac{\delta_t + \delta_c + \delta_v}{h_e} = \frac{M}{h_e^2}\left(\frac{1}{K_t} + \frac{1}{K_{cf,c}} + \frac{1}{K_{cw,v}}\right) \tag{12}$$

The initial rotational stiffness of the prefabricated RCS joint can be expressed as

$$K_i = \frac{M}{\theta} = \frac{h_e^2}{\frac{1}{K_t} + \frac{1}{K_{cf,c}} + \frac{1}{K_{cw,v}}} \tag{13}$$

The skeleton curve obtained from the test is smooth, and in this paper, a polyline was adopted to represent it. The flexural rigidity in the polyline model approximates the tangent stiffness $K_h = K_i/\eta$ of the curve, where K_i is the initial rotational stiffness and η is the influence coefficient, the recommended value of η is 1.5, i.e., $K_h = K_i/1.5$. The stiffness of the approximation is $K_p = 0.1K_h$, and the stiffness of the descending section is approximately $K_a = -0.2K_h$. The yield moment can be approximated by $M_y = 0.85M_u$.

The above method was adopted to calculate the prefabricated RCS joint in the test, and the initial stiffness (K_i) was 23,668 kN·m/rad, and the ultimate bending moment (M_u) was 197 kN·m. The calculated values of the key points of the tri-linear skeleton curve model are shown in Table 1.

The calculated tri-linear skeleton curve and the test curve are shown in Fig. 11. It can be seen that the tri-linear skeleton curve is consistent with the test curve, indicating the feasibility and accuracy of the theoretical model.

3.2. Hysteresis rules

At the beginning of loading, the semi-rigid prefabricated RCS joint is basically in the elastic stage, and the curves of each hysteresis loop during loading and unloading coincided with each other. The specimens enter the non-linear stage after yielding, the residual deformation increases with the increasing load displacement. The overall hysteresis curve is bowed and appears to be full, which indicates that the endplate connection has a good energy dissipation capacity and the joint can absorb a large amount of seismic energy.

According to the load-unload-reload track in the moment-rotation hysteresis curve, for the prefabricated RCS joint, it can be found that the restraint stiffness of unloading is slightly smaller than the initial stiffness, but it can be roughly considered to be equal to the convenience of calculation. During unloading, when passing through the horizontal axis, the descent curve follows the tangent direction of the reverse loading curve. Therefore, the hysteresis rule in the classical Takeda model was adopted [31]. The hysteresis rule belongs to the maximum point-directed type, i.e. during the loading, it always points to the maximum point of the last loading.

3.3. Model verification

To simulate the prefabricated RCS joint, the SAP2000 software was employed. The nonlinear connection element was adopted to consider the semi-rigid mechanical behavior of the joint [32,33], as shown in Fig. 12. The geometric dimensions of the numerical model are the joint

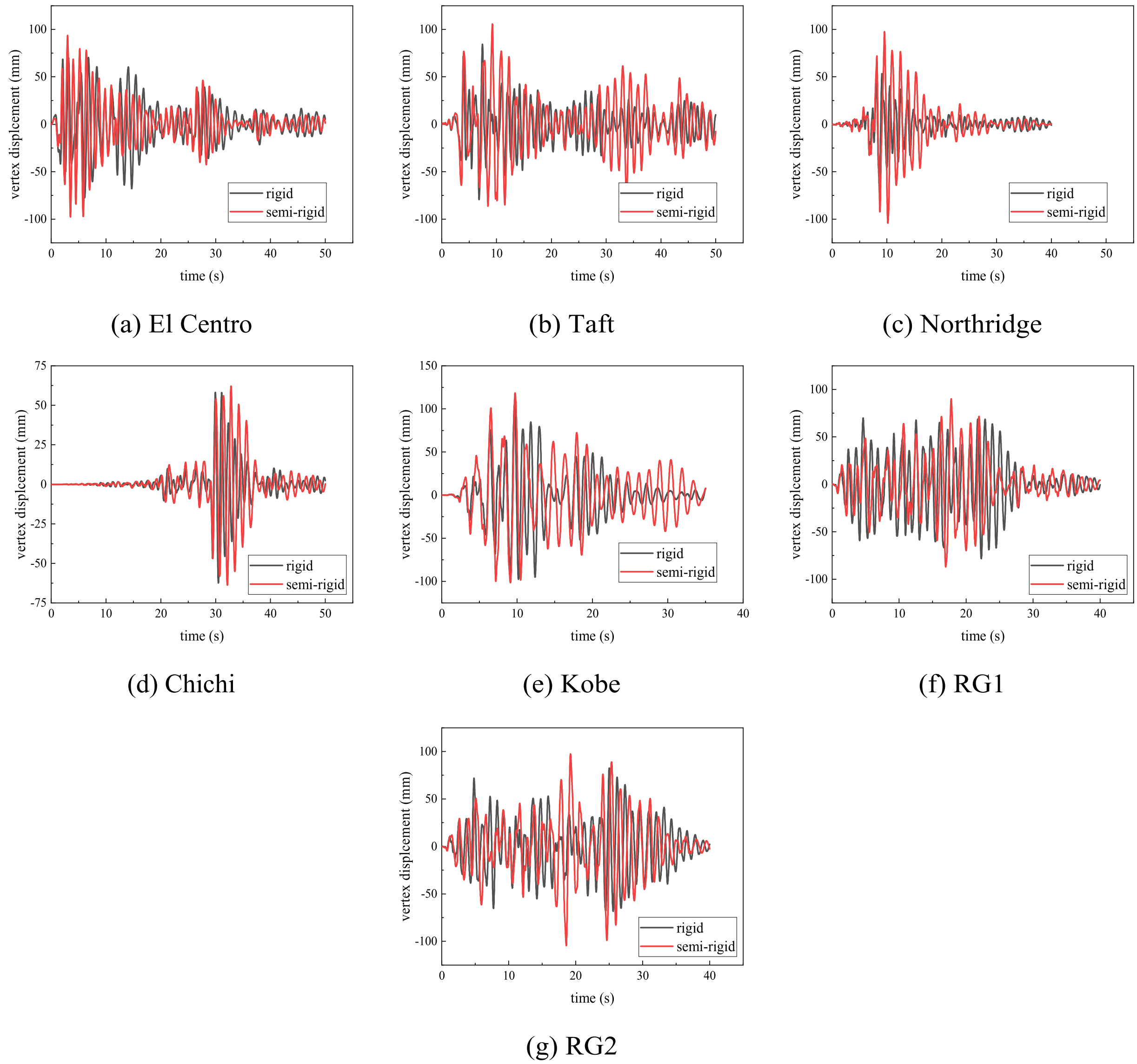

Fig. 17. Top displacement.

Table 4
Maximum top floor displacement of frames under earthquake.

No.	Seismic waves	Maximum displacement /mm		$(\Delta_2 - \Delta_1)/\Delta_1$
		rigid (Δ_1)	semi-rigid (Δ_2)	
1	El Centro	77.64	97.70	25.8 %
2	TAFT	79.32	86.35	8.9 %
3	Northridge	71.45	104.22	45.9 %
4	Chichi	62.47	63.77	2.1 %
5	Kobe	97.59	101.54	4.1 %
6	RG1	78.35	90.01	14.9 %
7	RG2	82.49	104.24	26.4 %

specimen.

The values in Table 1 were input into the connection element. The Takeda hysteresis model in SAP2000 was selected. The comparison between the experimental value and the simulation results is shown in Fig. 13. The comparison indicates that the proposed moment-rotation hysteresis model can well simulate the hysteresis behavior of the semi-rigid RCS joint.

4. Seismic analysis of the prefabricated RCS frame

4.1. Example model

A 5-story RCS frame structure was designed as the basic analysis model, its fortification intensity is 7 degrees, the design seismic acceleration is 0.10 g, and the site characteristic period is 0.4 s. The load of the floor and roof is 4.5 kN/m^2, and the live load is 2 kN/m^2.

The design process of the semi-rigid RCS structure was as follows: firstly, the elastic base shear of the structure and the yield base shear for plastic design was determined according to the design response spectrum. Then, the distribution of seismic activity along the story height was determined according to the lateral force distribution model. The size of the beam and the column was preliminarily selected, the bearing capacity of the semi-rigid connection was designed, and the bending capacity of the steel beam was checked. Finally, the axial force and bending moment of each floor column were determined, and the reinforcement design of the concrete column was carried out. The structural plan and elevation of the frame are shown in Fig. 14(a) and Fig. 14(b), respectively. The height of the RCS frame is 3.3 m. Steel beams and endplates are made of Q235 steel, concrete columns are made of C30 concrete, longitudinal reinforcement is HRB335 and hoop reinforcement

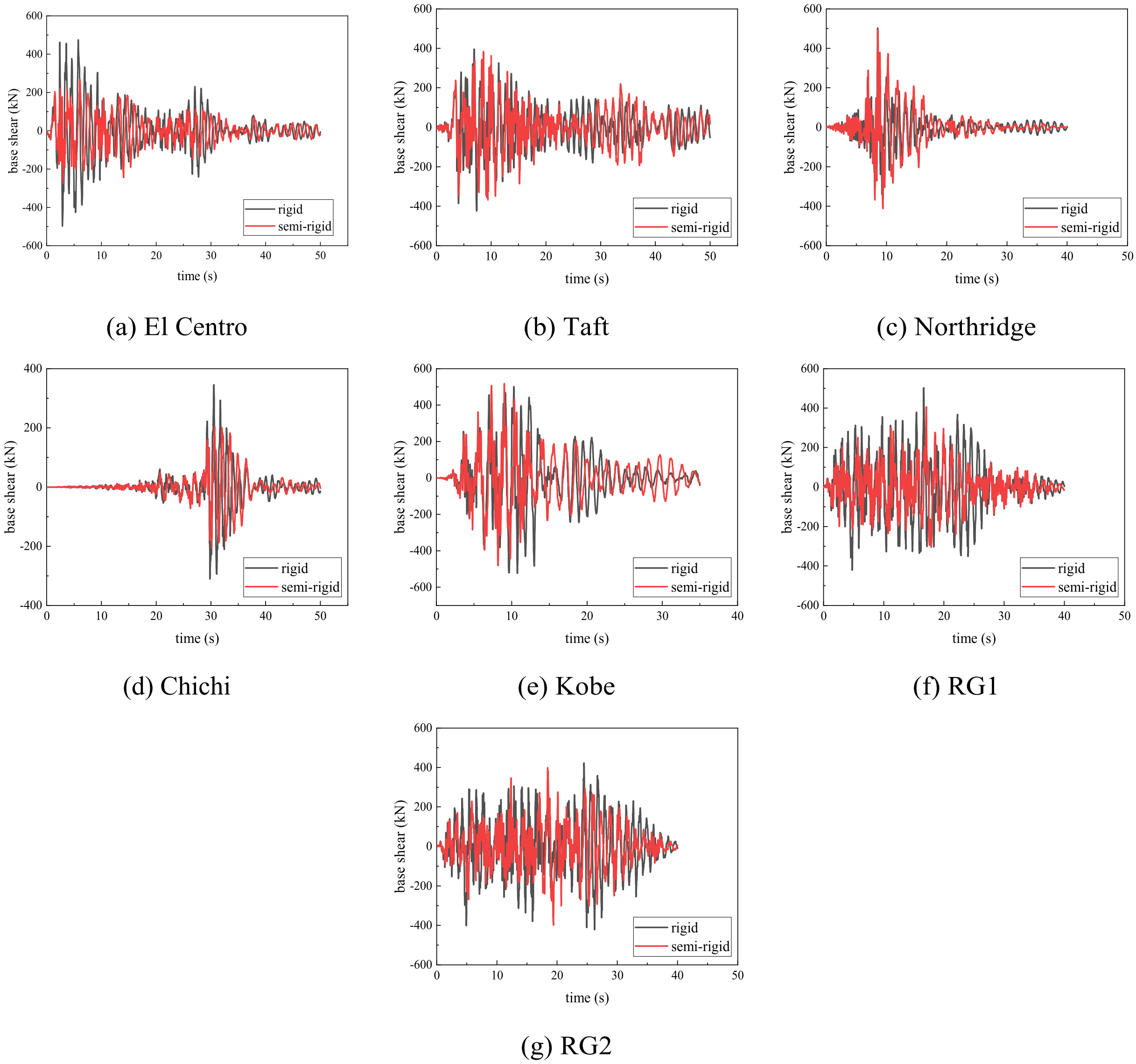

Fig. 18. Base shear.

Table 5
Maximum base shear of frames under earthquake.

No.	Seismic waves	Maximum base shear / kN		$(F_2 - F_1)/F_1$
		rigid (F_1)	semi-rigid (F_2)	
1	El Centro	497.04	270.01	−45.7 %
2	TAFT	423.98	383.50	−9.5 %
3	Northridge	502.19	492.94	−1.8 %
4	Chichi	344.84	204.34	−40.7 %
5	Kobe	523.81	516.89	−1.3 %
6	RG1	502.31	405.23	−19.3 %
7	RG2	423.10	399.04	−5.7 %

is HPB300.

In the analytical model, the column section size is 550 × 550 mm, the beam is HN300 × 160 × 8 × 12 mm, and the endplate is 450 × 160 × 9 mm. In the rigid RCS model, the plastic hinge curve of the steel beam was defined by FEMA356. In the semi-rigid prefabricated RCS model, the semi-rigid connection was determined by the tri-linear model mentioned above, and the contrast curves are shown in Fig. 15.

4.2. Modal analysis

The modal analysis of semi-rigid and rigid RCS structures was carried out. The first six orders of the natural vibration periods of the structure are shown in Table 2. The vibration modes of the structure are shown in Table 3.

From the results, the semi-rigid connection reduces the stiffness of the structure and increases the vibration period of the structure. Besides, it has a great influence on the low-order mode periods and has a gradually decreasing effect on the high-order mode periods.

4.3. Dynamic elastic–plastic analysis

To further investigate the effect of semi-rigid connections on the seismic performance of RCS structures, a dynamic elastic–plastic analysis of the structure was performed [34]. According to the code for seismic design of buildings [35], seven ground motions were selected, including five real ground motions and two synthetic ground motions. All the ground motions were scaled to a peak ground acceleration (PGA) of 220 cm/s^2, seven ground motions were El Centro wave, Taft wave, Northridge wave, Chichi wave, Kobe wave, RG1, RG2 respectively. The seismic influence coefficient of the design basis earthquake and the

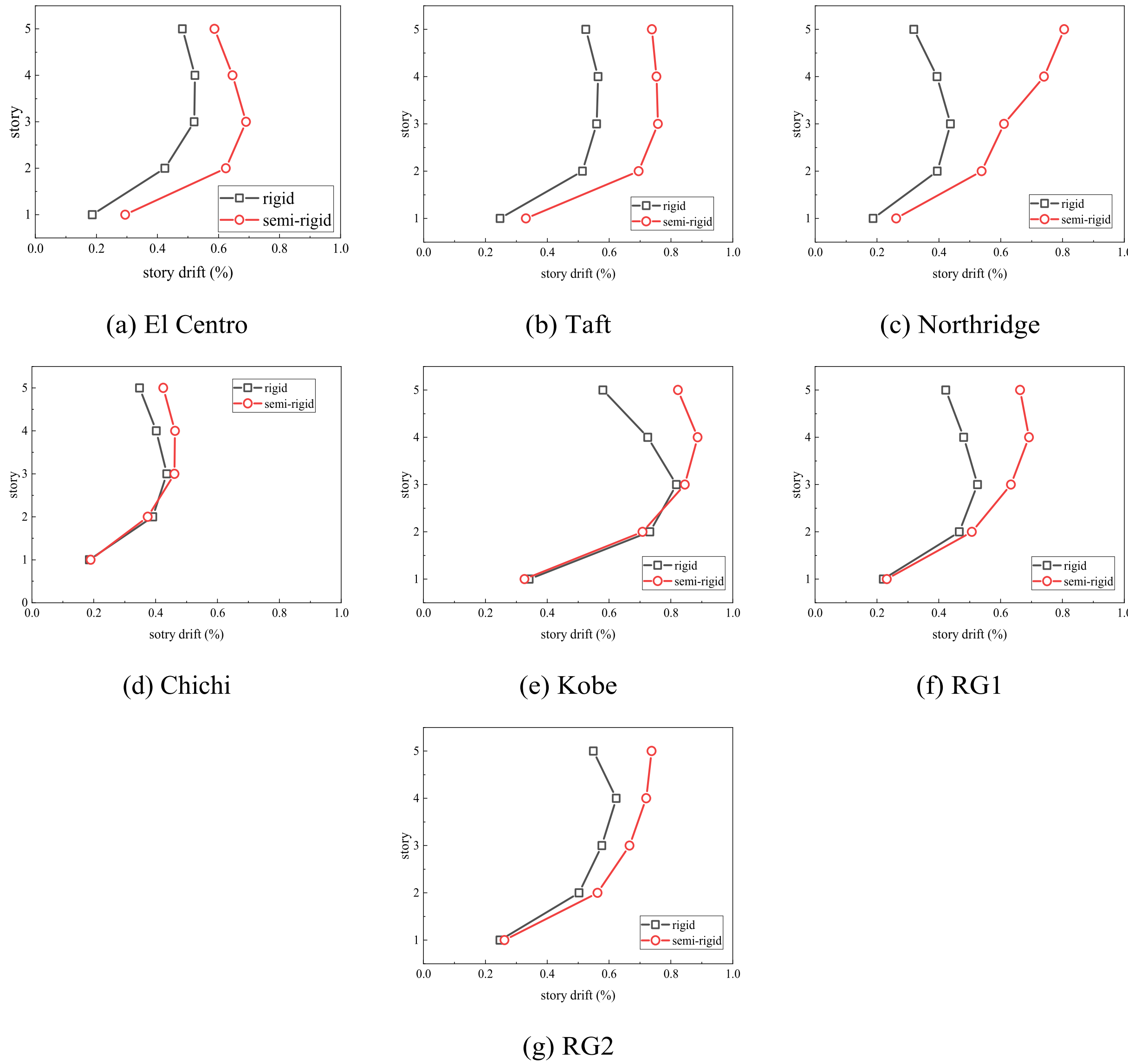

Fig. 19. The maximum inter-story drift angles.

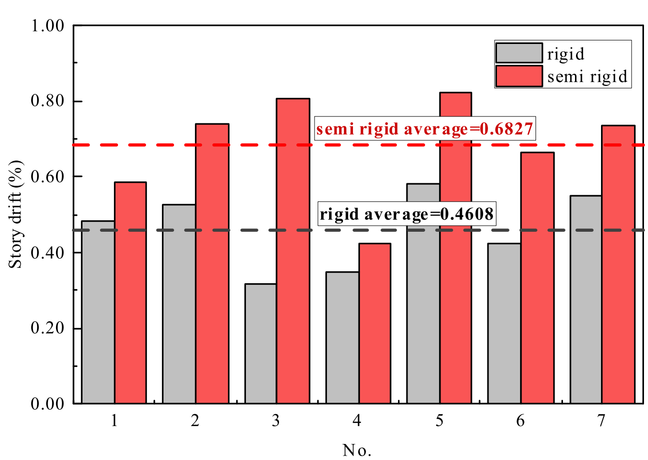

Fig. 20. Comparison chart of maximum inter-story drift angles.

seven ground motion records are shown in Fig. 16.

The relationship between vertex displacement and time of rigid and semi-rigid RCS frames under 7 ground motions is shown in Fig. 17. The maximum top floor displacement of rigid and semi-rigid RCS frames under different ground motions is shown in Table 4.

The base shear of rigid and semi-rigid RCS frames under different ground motions are shown in Fig. 18 and Table 5.

The maximum inter-story drift angles of rigid and semi-rigid RCS frames under different seismic waves are shown in Fig. 19 and Fig. 20.

According to the comparison results, the top displacement time history curve and the base shear time history curve of rigid and semi-rigid RCS frames are roughly the same in the seven wave cases. The semi-rigid connection can effectively reduce the base shear of the RCS structure by up to 45.7%. Due to the reduction of structural stiffness, the top displacement and the maximum inter-story drift angle of the semi-rigid RCS structure are larger than the rigid frame. Under rare earthquakes, the maximum inter-story drift angle of the semi-rigid RCS frame increases by 32.5% on average compared with that of the rigid frame, but still meets the code requirement of less than 1/50.

5. Conclusions

Through the test of the prefabricated RCS joint and the seismic analysis of the semi-rigid RCS structure, the conclusions are summarized as follows:

(1) Due to the construction of the steel jacket, the joint core area can be approximated as a rigid connection. The extended beam of the embedded part is connected to the structure through endplates and bolts, which can realize the prefabrication and control the plastic hinge to appear at the connecting position. The hysteretic curve of the joint is a full shuttle shape, indicating it has a good energy dissipation capacity and ductility.
(2) The theoretical moment-rotation model proposed in this paper, i. e., the tri-linear skeleton curve, combined with the Takeda hysteresis rule, can be used to accurately calculate and simulate the moment-rotation hysteresis curve of the semi-rigid prefabricated RCS joint.
(3) For semi-rigid prefabricated RCS structures, due to the decrease of the connection stiffness, the overall stiffness of the structure is reduced. Compared with the rigid RCS structure, the natural vibration periods of the semi-rigid RCS structure increase. Under the same seismic action, the base shear force of the semi-rigid RCS structure is smaller than that of the rigid RCS structure, and the maximum inter-story drift angles and top displacement will increase, but still meet the requirements of the seismic code.

Declaration of Competing Interest

The authors declare that they have no known competing financial interests or personal relationships that could have appeared to influence the work reported in this paper.

Acknowledgments

The authors gratefully acknowledge the financial support provided by the National Natural Science Foundation of China (No.51978316), Research and Innovation Plan for Postgraduates in Jiangsu Province (No.SJCX20_1476).

References

[1] Parra-Montesinos GJ, Liang X, Wight JK. Towards deformation-based capacity design of RCS beam–column connections. Eng. Struct. 2003;25(5):681–90. https://doi.org/10.1016/S0141-0296(02)00177-3.
[2] Bugeja MN, Bracci JM, Moore Jr WP. Seismic behavior of composite RCS frame systems. J. Struct. Eng. 2000;126(4):429–36. https://doi.org/10.1061/(ASCE)0733-9445(2000)126:4(429).
[3] Alizadeh S, Attari NKA, Kazemi MT. Experimental investigation of RCS connections performance using self-consolidated concrete. J. Constr. Steel Res. 2015;114:204–16. https://doi.org/10.1016/j.jcsr.2015.07.026.
[4] Mirghaderi SR, Eghbali NB, Ahmadi MM. Moment-connection between continuous steel beams and reinforced concrete column under cyclic loading. J. Constr. Steel Res. 2016;118:105–19. https://doi.org/10.1016/j.jcsr.2015.11.002.
[5] R. Kanno, G.G. Deierlein, Design model of joints for RCS frames[C]. Composite construction in steel and concrete. 2002: 947-958. 10.1061/40616(281)82.
[6] Sheikh TM, Deierlein GG, Yura JA, Jirsa JO. Beam-column moment connections for composite frames: Part 1. J. Struct. Eng. 1989;115(11):2858–76.
[7] Alizadeh S, Attari NKA, Kazemi MT. The seismic performance of new detailing for RCS connections. J. Constr. Steel Res. 2013;91:76–88. https://doi.org/10.1016/j.jcsr.2013.08.010.
[8] Nguyen XH, Nguyen Q-H, Le DD, Mirza O. Experimental study on seismic performance of new RCS connection. Structures. Elsevier 2017;9:53–62.
[9] Doost RB, Khaloo A. Steel web panel influence on seismic behavior of proposed precast RCS connections. Structures. Elsevier 2021;32:87–95. https://doi.org/10.1016/j.istruc.2021.02.057.
[10] Zhang X, Zhang J, Gong X, Zhang S. Seismic performance of prefabricated high-strength concrete tube column–steel beam joints. Adv. Struct. Eng. 2018;21(5):658–74.
[11] Pan Z, Si Qi, Zhou Z, Zhang Y, Zhu Y, Chen X. Experimental and numerical investigations of seismic performance of hybrid joints with bolted connections. J. Constr. Steel Res. 2017;138:867–76.
[12] Si Q, Pan Z. Numerical study on performance of prefabricated RCS joint under normal temperature and fire. KSCE J. Civ. Eng. 2021;25(11):4322–34. https://doi.org/10.1007/s12205-021-2118-y.
[13] Tartaglia R, D'Aniello M, Rassati GA. Proposal of AISC-compliant seismic design criteria for ductile partially-restrained end-plate bolted joints. J. Constr. Steel Res. 2019;159:364–83. https://doi.org/10.1016/j.jcsr.2019.05.006.
[14] Lu S, Wang Z, Pan J, Wang P. The Seismic Performance Analysis of Semi-rigid Spatial Steel Frames Based on Moment-Rotation Curves of End-plate Connection. Structures. Elsevier 2022;36:1032–49.
[15] Tartaglia R, D'Aniello M, Landolfo R. The influence of rib stiffeners on the response of extended end-plate joints. J. Constr. Steel Res. 2018;148:669–90. https://doi.org/10.1016/j.jcsr.2018.06.025.
[16] Cai Z-W, Liu X, Li L-Z, Lu Z-D, Chen Yu. Seismic performance of RC beam-column-slab joints strengthened with steel haunch system. J. Build. Eng. 2021;44:103250.
[17] Zhang Z-Y, Ding R, Nie X, Fan J-S. Seismic performance of a novel interior precast concrete beam-column joint using ultra-high performance concrete. Eng. Struct. 2020;222:111145.
[18] Ning N, Qu W, Ma ZJ. Design recommendations for achieving "strong column-weak beam" in RC frames. Eng. Struct. 2016;126:343–52. https://doi.org/10.1016/j.engstruct.2016.07.053.
[19] Ataei A, Bradford MA, Valipour HR. Moment-rotation model for blind-bolted flush end-plate connections in composite frame structures. J. Struct. Eng. 2015;141(9):04014211. https://doi.org/10.1061/(ASCE)ST.1943-541X.0001147.
[20] Shi YJ, Chan SL, Wong YL. Modeling for moment-rotation characteristics for end-plate connections. J. Struct. Eng. 1996;122(11):1300–6. https://doi.org/10.1061/(ASCE)0733-9445(1996)122:11(1300).
[21] Lee SS, Moon TS. Moment–rotation model of semi-rigid connections with angles. Eng. Struct. 2002;24(2):227–37. https://doi.org/10.1016/S0141-0296(01)00066-9.
[22] Kong Z, Kim SE. Moment-rotation model of single-web angle connections. Int. J. Mech. Sci. 2017;126:24–34. https://doi.org/10.1016/j.ijmecsci.2017.03.008.
[23] Tartaglia R, D'Aniello M, Zimbru M. Experimental and numerical study on the T-Stub behaviour with preloaded bolts under large deformations. Structures. Elsevier 2020;27:2137–55. https://doi.org/10.1016/j.istruc.2020.08.039.
[24] Shi G, Shi Y, Wang Y, Bradford MA. Numerical simulation of steel pretensioned bolted end-plate connections of different types and details. Eng. Struct. 2008;30(10):2677–86.
[25] Tartaglia R, D'Aniello M, Rassati GA, Swanson JA, Landolfo R. Full strength extended stiffened end-plate joints: AISC vs recent European design criteria. Eng. Struct. 2018;159:155–71.
[26] Chen X, Shi G. Calculation of moment-rotation curves of ultra-large capacity end-plate connections based on component method. Eng. Mech. 2017;34(5):30–41. in Chinese.
[27] Tartaglia R, D'Aniello M, Zimbru M. Experimental and numerical study on the T-Stub behaviour with preloaded bolts under large deformations. Structures. Elsevier 2020;27:2137–55. https://doi.org/10.1016/j.istruc.2020.08.039.
[28] Zhang Y, Gao S, Guo L, Qu J, Wang S. Ultimate tensile behavior of bolted T-stub connections with preload. J. Build. Eng. 2022;47:103833.
[29] Standard B. Eurocode 3-Design of steel structures. BS EN 1993-1, 2006, 1: 2005.
[30] Li G, Duan L, et al. Initial rotational stiffness of H-shaped beams to RHS column end-plate connections using blind bolts. J. TongJi Univ. (Natural Science) 2018;46(05):565–73. in Chinese.
[31] Roufaiel MSL, Meyer C. Analytical modeling of hysteretic behavior of RC frames. J. Struct. Eng. 1987;113(3):429–44. https://doi.org/10.1061/(ASCE)0733-9445(1987)113:3(429).
[32] Nazri FM, Ken PY. Seismic performance of moment resisting steel frame subjected to earthquake excitations. Front. Struct. Civil Eng. 2014;8(1):19–25. https://doi.org/10.1007/s11709-014-0240-3.
[33] Galal MA, Bandyopadhyay M, Banik AK. Dual effect of axial tension force developed in catenary action during progressive collapse of 3D composite semi-rigid jointed frames. Structures 2019;19:507–19. https://doi.org/10.1016/j.istruc.2019.02.006.
[34] Tartaglia R, D'Aniello M, Landolfo R. Seismic performance of Eurocode-compliant ductile steel MRFs. Earthquake Eng. Struct. Dyn. 2022. https://doi.org/10.1002/eqe.3672.
[35] GB50011-2010 Code for Seismic Design of Buildings. Beijing: China Architecture & Building Press, 2016. (in Chinese).